Cement and Concrete Composites 145 (2024) 105316

Contents lists available at ScienceDirect

Cement and Concrete Composites

journal homepage: www.elsevier.com/locate/cemconcomp

Role of delignified and lignin-containing cellulose nanofibers in enhancing durability performances of portland cement composites

Nithya Nair [a], Muhammad Intesarul Haque [a], Salman Siddique [a], Rakibul I. Khan [b], Warda Ashraf [a,*], Keith Gourlay [c], Surendra Shah [a]

[a] Department of Civil Engineering, University of Texas at Arlington, Nedderman Hall, Arlington, TX, 76010, USA
[b] Laticrete International, Inc., Bethany, CT, 06524-3423, USA
[c] Performance BioFilaments, Vancouver, BC, V6T 1Z4, Canada

ARTICLE INFO

Keywords:
Cellulose nanofibers
Sulfate attack
Cement
Alkali silica reaction
Durability

ABSTRACT

This study investigates the effectiveness of cellulose nanofibers (CNF) in enhancing the long-term durability performance of ordinary portland cement (OPC) composites against sulfate attack and alkali-silica reaction (ASR). Two different types of cellulose nanofibers, namely lignin-containing cellulose nanofibers (LCNF) and delignified cellulose nanofibers (DCNF), were used in three different dosages (0.05%, 0.1%, and 0.3% by weight of the cement) to produce mortar samples. The heat of hydration and microstructural studies confirmed that none of the selected CNFs negatively affected the early-age cement hydration. Dynamic vapor sorption (DVS) isotherms revealed that the addition of CNF increased the amounts of C–S–H of the paste samples and therefore, resulted in the densification of the matrix. LCNF and DCNF-containing mortar samples were exposed to 5% $MgSO_4$ and 5% Na_2SO_4 for 6 months. The results showed that incorporating CNF improved the resistance of mortar against sulfate attack. Specifically, after 6 months of sulfate exposure, the compressive strengths of the control samples were reduced by nearly 50%. In the case of 0.3% DCNF and 0.3% LCNF-containing batches, the strength reductions were less than 20% after the same sulfate exposure duration. Moreover, the expansion due to the ASR of CNF-containing mortar bars was nearly 97% lower than the samples without CNF after one year of exposure test. For all the tested parameters, LCNF-containing samples showed better performance compared to DCNF-containing samples.

1. Introduction

There has been a notable increase in interest surrounding the utilization of alternative materials for the development of cementitious composites that offer improved mechanical performance and durability with reduced CO_2 emissions [1,2]. Among these materials, nanomaterials have a significant impact on improving the mechanical and durability properties of cement-based materials. The unique properties of nanomaterials, such as their high surface area to volume ratio and increased reactivity, make them highly effective at enhancing the performance of cementitious composites [3–6]. When incorporated into cementitious composites, nanomaterials can improve several properties such as compressive strength, tensile strength, flexural strength, fracture toughness, and durability against various types of environmental degradation [5,7]. Additionally, nanomaterials were also found to impart some special characteristics into cement composites, such as self-cleaning with self-sensing [8,9] and neutron shielding [10,11]. However, the relatively high cost of nanomaterials often limits their commercial applications to develop cementitious composites [12,13].

The cellulose-based nanomaterials extracted from plants are an advantageous raw material due to their low cost, renewable nature, and low carbon footprint [14]. The cellulose-based materials have a significant range of structural forms, such as nano-fibrillated cellulose [15], cellulose nanocrystals [16], microcrystalline cellulose [17], and cellulose nanofibers [18]. Their chemical as well as physical structure depends on their source and production method. Cellulose nanofibers (CNF), due to their ease of production, have been used in various studies to show their influence on cement hydration and strength development [19,20]. It has been reported that CNF can promote the hydration of cement composites [21]. The use of CNF in low dosages helped in improving the mechanical properties of cement composites [21–24]. Cellulose microfibers have also been conventionally employed as

* Corresponding author.
E-mail address: warda.ashraf@uta.edu (W. Ashraf).

https://doi.org/10.1016/j.cemconcomp.2023.105316
Received 18 June 2023; Received in revised form 17 September 2023; Accepted 5 October 2023
Available online 5 October 2023

reinforcing agents in cement-based composites [25,26]. Earlier research has demonstrated that the incorporation of nanocellulose can control plastic shrinkage and improve strengths of concrete [27,28].

However, a relatively large dosage of CNF can reduce the compressive strengths of the cementitious composites [29]. Besides, incorporating these cellulose nanomaterials into cement-based materials can offer several multifunctional benefits, including the ability to perform internal curing [21,30]. The use of CNF resulted in lower penetration of sulfate ions when exposed to Na_2SO_4 [31]. It was concluded that the use of CNF in Type 1 Portland cement improves the resistance to sulfate attack similar to that of the specially formulated sulfate resistance cement [31]. In another study, Goncalves et al. recorded that the use of CNF restricted the penetration of chloride ions into the cement matrix [32].

The damage and deterioration in structures exposed to sulfate attack lead to premature cracking and reduced service life [33]. The structures can be exposed to sulfate ions from soil, industrial discharges, and coastal area water. The sulfate attack results in structural deformity caused by volume expansion, cracking, and spalling of cement. The serious damages caused by sulfate attacks on cement-based composites have been studied in detail to formulate eco-friendly and durable structures with enhanced service life [34–36]. In that regard, the present study was designed to assess the impact of CNF on the durability of mortar exposed to sulfate attacks. Compared to a previous study conducted by Goncalves et al. [31], the present experimental program considers two different forms of CNFs namely lignin-containing cellulose nanofibers (LCNF) and delignified cellulose nanofibers (DCNF). Moreover, it has been well established that the ingress of $MgSO_4$ is more detrimental to cement composites as compared to Na_2SO_4 ingress [37]. To provide a comprehensive analysis, both $MgSO_4$ and Na_2SO_4 solutions were used to mimic sulfate attack in this study. In addition to sulfate attacks, this study also evaluated the role of LCNF and DCNF in enhancing the resistance of mortar samples against alkali-silica reaction (ASR). For this purpose, various mortar specimens were fabricated by adding LCNF or DCNF at 0.05%, 0.1%, and 0.3% by weight of the cement. The ASR expansion measurement was carried out by considering reactive borosilicate aggregates and observations were taken up to one year.

2. Experimental details

2.1. Materials

Portland cement conforming to guidelines of ASTM C150 [38] Type 1 was used as the binder. Standard sand conforming to ASTM C778 [39] was used as the fine aggregate. LCNF and DCNF samples were supplied by the Performance Biofilaments, Inc. (Canada). The LCNF fibrils are produced from unbleached Kraft pulp. Since these fibers are unbleached, residual lignin is present during the fibrillation process. On the other hand, DCNF is produced from delignified (bleached) Kraft pulp, which has had the lignin removed. The presence of lignin can significantly affect the properties and efficiency of CNF production. Several studies reported that the presence of lignin can reduce the energy consumption of mechanical fibrillation and improve the yield of LCNF [40]. Additionally, lignin deposits on fiber surface as nanoparticles, resulting in a very high surface area [40]. During the fibrillation process, once the fiber structure is broken, the antioxidant effect and physical barrier of lignin can prevent fiber from re-aggregation and facilitate the fibrillation of cellulose into fine diameters [40]. Such process results in finer and uniform fiber distribution in LCNF compared to DCNF [40]. Table 1 presents the chemical composition of cement. The properties of CNFs are listed in Table 2. Fig. 1 shows the SEM (dried sample) and TEM (dispersed sample) images of LCNF and DCNF. It is visible that both types of CNF have a fibrous structure with an elongated form entangled within the same fibers. The LCNF and DCNF had thick slurry like consistence with solid contents 29% and 34% in water, respectively. To maintain the appropriate water-cement ratio, the amount of free water present in the cellulose was subtracted from the total amount of water required.

2.2. Sample preparation

Table 3 shows the formulations of mortar containing LCNF and DCNF. CNFs were added in terms of 0.05%, 0.1%, and 0.3% by weight of cement. These CNFs were first mixed in water by using a high-shear blender for 3 min. Such a dispersion method was previously reported in Ref. [41] for the similar types of CNF and recommended by the supplier. The workability of the mixes with the addition of CNF was drastically reduced. Fig. 2 shows the flow diameter measurements as per the ASTM C230 of the mortar samples with and without CNF. The flow diameter was reduced by nearly 50% and 100% with the addition of 0.05% and 0.3% CNF, respectively. Both DCNF and LCNF showed similar reductions in the workability of mortar samples. Such reductions in workability were expected due to the high-water absorption capacity of CNF.

The mortar samples for sulfate exposure conditions were prepared as per the guidelines of ASTM C1012 [42]. The water-to-cement ratio (w/c) was kept at 0.485 for all the mortar bar mixes and 0.42 for the cube mixes. Table 3 shows the mix proportions of the mortar samples. After casting, the samples were kept in sealed condition for 24 h. Mortar samples were cast into 50 mm cube molds for compressive strength measurements. For length change measurements, prism samples of the dimensions 25 mm × 25 mm × 250 mm were cast. The samples were then de-molded and kept for further curing in a sealed condition for 28 days. After 28 days of curing, the samples were exposed to 5% $MgSO_4$ and 5% Na_2SO_4 solution for up to 180 days. The sample strengths were tested after 15, 30, 60, 90, and 180 days of exposure. The sulfate solution was replenished at every testing duration to maintain the concentration of sulfate ions. For microstructural investigations, paste specimens were cast and exposed to the same sulfate solution. The microstructural samples were collected at due time and were vacuum treated with isopropanol to stop further reactions.

For the resistance to ASR, Type 33 alkali-borosilicate glass provided by NBS, Vitro minerals were used to act as the reactive aggregate. The guidelines of ASTM C1260 [43] were used to prepare the mortar samples and exposure to environmental conditions. Specifically, mortar samples submersed in 1 N NaOH solution at a temperature of 80 °C. After this duration, the samples were kept in the same solution, but at room temperature, and the length changes were monitored for up to one year.

2.3. Test procedures

The heat of hydration was monitored using a commercially available isothermal calorimeter (TAM air by TA instrument). The paste samples were placed inside the calorimeter chamber immediately after mixing

Table 1
Chemical composition (wt.%) of the raw materials.

Raw material	Mass fraction w/%						
	Al_2O_3	SiO_2	CaO	Fe_2O_3	MgO	SO_3	K_2O
Cement	3.87	21.2	65.3	3.10	0.816	4.28	0.679

Table 2
Properties of cellulose nanofibers.

Fibril Diameter	80–300 nm
Fibril length	100–500 μm
Aspect ratio	800–1000 L/D
Surface area	80,000 m^2/kg
Density	0.5 g/cm^3

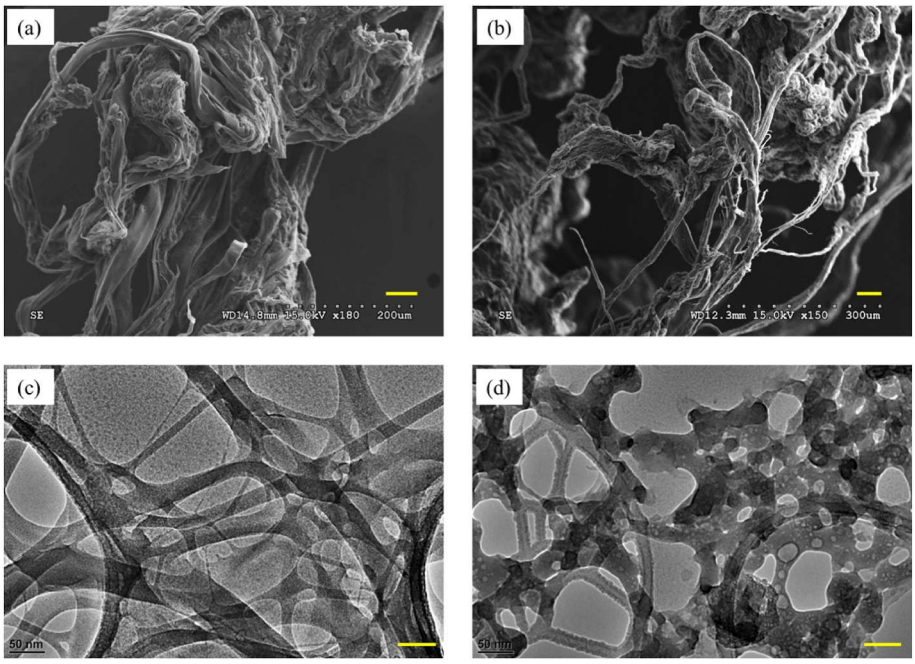

Fig. 1. Scanning electron microscopic (SEM) images of cellulose nanofibers, (a) LCNF, (b) DCNF and transmission electron microscopic (TEM) images of cellulose nanofibers, (c) LCNF, (d) DCNF. Scale bar represents 50 μm.

Table 3
Mix proportions (kg/m^3).

Mix id	Cement	Sand	Water	CNF slurry (contains CNF and free water)
Control	545.45	1500	264.39	0
0.05% DCNF	545.45	1500	264.02	0.80
0.1% DCNF	545.45	1500	263.48	1.61
0.3% DCNF	545.45	1500	261.37	4.81
0.05% LCNF	545.45	1500	263.89	0.92
0.1% LCNF	545.45	1500	263.23	1.86
0.3% LCNF	545.45	1500	260.61	5.56

and the signals were corrected after 45 min. The heat of hydration was measured up to 90 h at 23 °C. The isothermal calorimetry was repeated for a few batches, and the standard deviations of the total heat measurements were less than 2%.

For thermogravimetry analysis (TGA), paste samples were first pulverized using mortar and pestle and passed through a #200 sieve. Approximately 30–40 mg sample was taken and put on the platinum pan of the TGA (commercially available TGA 550 by TA instrument). The sample was kept in the isothermal condition for 5 min at around 25 °C and the temperature was raised to 980 °C at a rate of 15 °C per minute afterward. To ensure an inert environment, nitrogen gas was purged into the chamber. TGA measurement can help indicate the decomposition of phases at temperature ranges. For example, the temperature range between 25 and 120 °C shows the decomposition of free water, ettringite, and C–S–H gel [44]. The decomposition of AFm phases is represented at 150–170 °C. Portlandite decomposition can be observed at 400–450 °C temperature range [44]. Calcium carbonate decomposition is observed at 600–850 °C temperature ranges [44]. Three replicate samples were initially tested through TGA to validate any deviation. Since the result deviations were less than 2% by weight, the TGA measurements were collected with only one sample for the remaining batches.

Powdered paste samples were also used for X-ray diffraction (XRD) measurements. XRD measurements were acquired on a Bruker D8 spectrometer using Cu Kα radiation (40 kV, 40 mA). The sample was scanned over a range of 5°–60°(2θ), using a step size of 0.01 per second.

Commercially available dynamic vapor sorption (DVS) equipment (Q 5000 by TA instruments) was used to obtain the sorption isotherms. The sample was first equilibrated at 97.5% RH for 5760 s. After this point, the RH was gradually reduced (with 5–10% RH steps) to obtain the desorption isotherm. The temperature was maintained constant (at 23 °C) during this experiment.

The compressive strength of the mortar cubes was measured following the ASTM C109 [45] method at 28 days of curing age and up to 180 days of sulfate exposure. The length change of the mortar bars

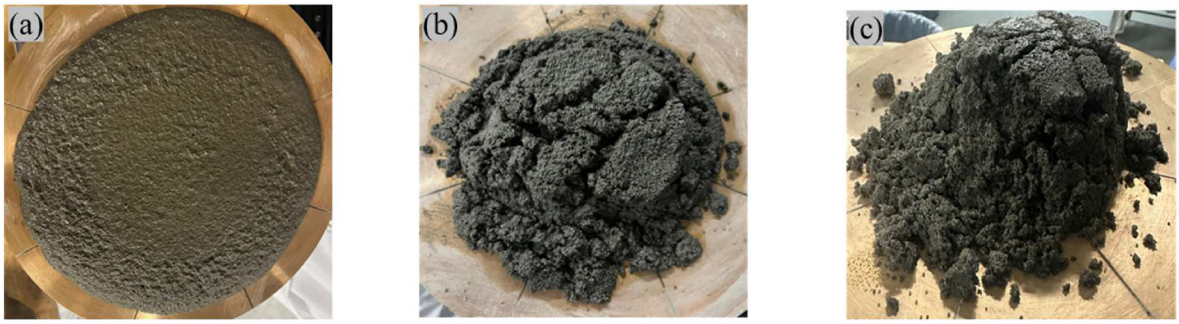

Fig. 2. Flow diameter measurements of mortar samples containing (a) 0% CNF, (b) 0.05% CNF, and (c) 0.3% CNF.

due to the sulfate exposure was measured following the specifications of ASTM C157 [46].

3. Results

3.1. Effects of LCNF and DCNF on hydrated cement paste and mortars

3.1.1. Effects on the compressive strengths

The compressive strengths of the mortar samples containing LCNF and DCNF after 28 days of curing are presented in Fig. 3. At 0.1% dosage, LCNF and DCNF-containing samples showed around a 10% increase in the 28-day compressive strength. The effects of both LCNF and DCNF on the compressive strengths were nearly the same. As discussed in a previously published article [23], the correlation between CNF dosage and cement hydration is non-linear. Such non-linear behavior was attributed to two competing mechanisms: (i) the negatively charged carboxyl groups can be adsorbed on unhydrated cement surface resulting in a delay of the hydration reaction, and (ii) due to the high surface area of CNF, it can also accelerate cement hydration due to the nucleation effect [23]. Based on the results of the experiment, it has been determined that dosages above or below 0.1% do not yield adequate performance. The lower compressive strengths at a higher dosage (0.3%) of LCNF and DCNF can be due to the agglomeration of fibers leading to the formation of weak zones in the cement matrix. Therefore, the 0.1% dose can be considered optimum for the mortar samples, which also matches our previous findings [24]. As such, while the durability performance of all the samples has been evaluated, microstructural evaluations only for the 0.1% CNF-containing specimens are presented in this article.

3.1.2. Effects on cement paste hydration and microstructure

The heat of hydration of the paste samples containing various dosages of CNF was monitored for 90 h and presented in Fig. 4. From the heat flow per g of cement (Fig. 4 a), it can be observed that the primary peak associated with cement hydration was shifted to the left due to the addition of CNF. This indicates all of the CNF accelerated the cement hydration. However, the effect of DCNF was more prominent in accelerating the cement hydration as compared to LCNF. The mix with 0.05% DCNF registered the highest heat flow rate and lowest dormant period. Among the LCNF mixes addition of 0.3% showed the highest heat flow. The CNF can act as nucleation sites for the formation of calcium silicate hydrate (C–S–H) thereby enhancing cement hydration in the acceleration stage. It should be noted that a few previous studies reported that the addition of CNF can lead to a lower cement hydration rate at the early stage [19,47]. It was reported that hydroxyl and carboxyl groups present in CNF binds with the calcium ions of cement limiting the nucleation sites for hydration [19]. Contradictorily, there are other articles that reported the cellulose nanomaterials can enhance the hydration of cement particles at an early age due to the nucleation effect (associated with the high surface area of CNF) [23]and later age by acting as water channels (addressed as “short-circuit diffusion”) [30]. In the present study, both LCNF and DCNF were primarily observed to improve cement hydration as evidenced by the increase in heat flow. Fig. 4 (b) shows the total heat release on the incorporation of LCNF and DCNF in cement mixes. Notably, both LCNF and DCNF registered higher early-age total heat as compared to the control but reach nearly the same total heat after around 90 h.

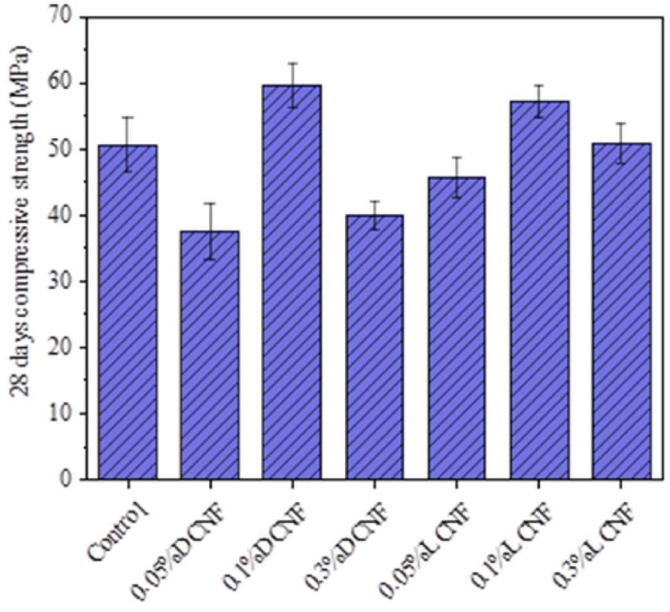

Fig. 3. Compressive strengths of mortar cubes after 28 days of sealed curing.

Fig. 5 shows the XRD spectra of control and CNF-containing specimens after 28 days of hydration in sealed curing conditions. The incorporation of CNF affected the traditional phases such as portlandite present in cement composites but did not lead to the formation of any new phases. An important observation is that both LCNF and DCNF specimens recorded relatively higher intensity of peaks for portlandite as compared to the control specimen. The higher portlandite formation indicates enhanced hydration of the CNF-containing batches after 28 days of sealed curing. The enhanced hydration due to the addition of a small dosage of CNF matches with the previously reported findings [24]. The intensity of the portlandite peak in LCNF-containing paste samples was higher than that of DCNF, indicating LCNF was more effective in enhancing hydration.

Fig. 6 shows the TGA plots of paste samples after 28 days of sealed curing. Like the XRD observations (Fig. 5), the LCNF and DCNF-containing specimens showed higher amounts of portlandite present as compared to the control specimen. However, the weight loss peak at around 150 °C due to the decomposition of C–S–H and Aft was higher for the control specimens as compared to CNF-containing specimens. Such reduced peak was attributed to lower ettringite formation in the samples containing CNF. As discussed in a previous study [21], the addition of CNF can reduce the amounts of ettringite formation in cement paste (without sulfate exposure) due to their ability to bind calcium ions. Based on the DTG curves in Fig. 6, the chemically bound water content was calculated within the temperature range of 110 °C to 550 °C, excluding the free water and carbonate content [44]. The higher chemically bound water content in the CNF-containing samples compared to the control batch indicate that the inclusion of CNF enhanced the degree of reaction.

The water vapor desorption isotherms of the paste samples are given in Fig. 7(a). The sorption isotherms were further analyzed as per the method proposed by Barrett, Joyner, and Halenda in 1951 (BJH method [48]). Due to the smaller molecular size of water compared to nitrogen and mercury, vapor sorption isotherms are often considered a preferred technique to understand the gel porosity and specific surface area (S_{BET}) measurement of the hydrated cementitious composites [49]. Here, specific surface area (S_{BET}) was calculated within the 35%–11% RH range of the vapor sorption isotherms by the BET method proposed by Brunauer, Emmett, and Teller [50]. As observed from Fig. 7, the S_{BET} was highest for 0.1% LCNF-containing paste followed by 0.1% DCNF and then the control batch. This trend matches with that observed in the case of portlandite contents during XRD and chemically bound water content from DTG/TGA measurements. Therefore, it can be confirmed that CNF-contained batches attained a higher degree of hydration compared to the control batch. Furthermore, LCNF-containing samples showed a higher degree of hydration compared to the DCNF sample. Considering the pore size distribution in Fig. 7(b), the DCNF containing sample showed higher porosity in the range of 2 nm–5 nm. On the other hand, the LCNF-containing sample showed higher porosity below 2 nm (to be specific at 1 nm). For hydrated cementitious materials, the pores

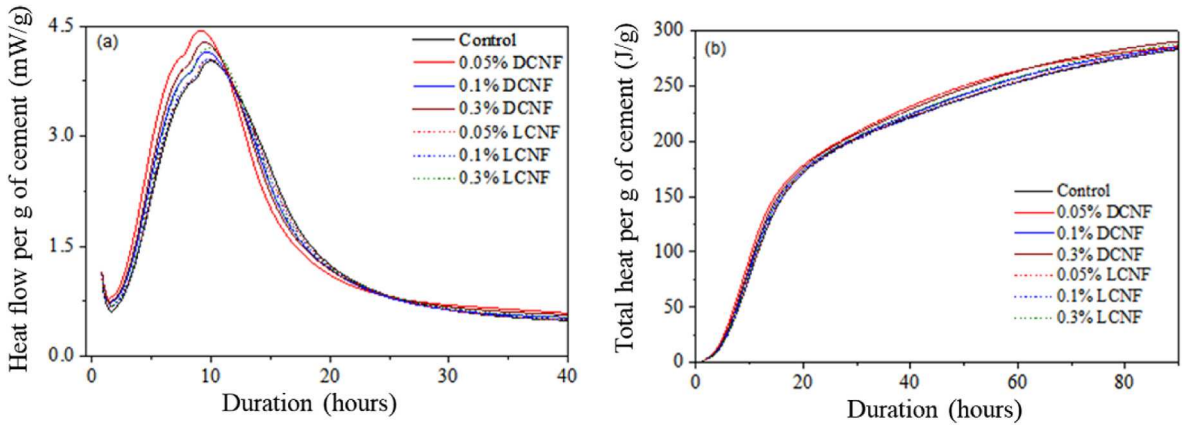

Fig. 4. Isothermal measurement of cement containing cellulose nanofibers: (a) Heat flow measurement, (b) Total heat per g of cement.

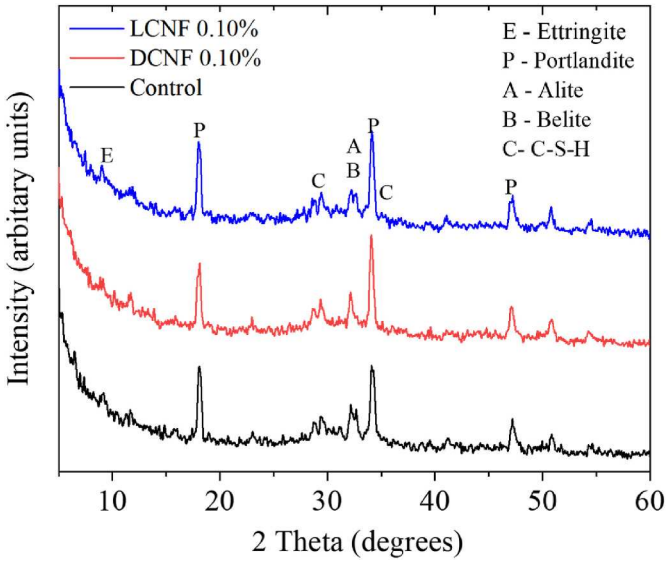

Fig. 5. XRD spectra of paste samples after 28 days of sealed curing.

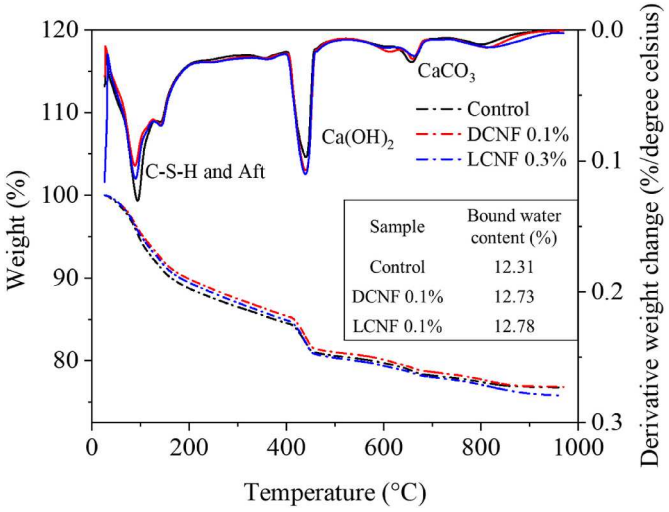

Fig. 6. Thermogravimetric analysis (TGA) plots of paste samples after 28 days of sealed curing.

sizes in the range of 2–5 nm are attributed to the pores between C–S–H gel clusters, more precisely between outer (or low-density) C–S–H [51]. Additionally, the pore sizes below 2 nm are attributed to the pores internal to the C–S–H clusters, and more specifically inner (or high density) C–S–H [51]. Therefore, while both types of CNF increased the C–S–H formation compared to the control sample, based on the pore size analysis, DCNF increased the low-density C–S–H and LCNF increased the high-density C–S–H contents.

3.2. Role of LCNF and DCNF in resisting damage induced by Na_2SO_4

3.2.1. Macroscale effects

Fig. 8 (a) and (b) shows the compressive strengths and length change (% expansion) of the mortar samples due to the exposure to Na_2SO_4 solution. After 6 months of exposure, all CNF-containing specimens registered higher compressive strength than that of the control specimen. 0.3% DCNF and 0.05% LCNF specimens registered the highest compressive strength among the specimens after 6 months of exposure. The % variation in the compressive strengths is given in Table 4. For the 0.1% DCNF and 0.1% LCNF specimens, the compressive strengths were 38.4% and 41.5% higher, respectively, than that of the control specimen. Furthermore, compared to the before-exposure condition, the compressive strength of the control batch dropped by nearly 47% after 6 months of exposure to Na_2SO_4. For 0.1% DCNF and 0.1% LCNF-containing batches, the decreases in strengths were −37% and −33%, respectively. For a few specimens (i.e., 0.3% DCNF and 0.05% LCNF), the compressive strengths were increased after sulfate exposure. These specimens showed relatively lower strength after 28 days of hydration, and strength may have increased due to the densification of the matrix during the sulfate exposure. The LCNF and DCNF specimens presented lower length change as compared to the control specimen when exposed to Na_2SO_4 solution. For a dosage of 0.1%, the LCNF specimen presented better dimensional stability as compared to DCNF specimens. In the case of a Na_2SO_4 attack, the sulfate ions react with portlandite and AFm phases present in a hydrated cement matrix and form gypsum and ettringite, which has an expansive nature. Formation of such expansive phases increases the internal stress in specimens leading to lower compressive strength. For the CNF-containing specimens, the matrix densification resulting from the enhanced hydration and the crack-bridging effects are the primary causes for better resistance to Na_2SO_4 attack.

3.2.2. Microscale effects

The sulfate attack caused by the ingress of Na_2SO_4 into the cement matrix leads to the conversion of portlandite to ettringite and gypsum. The XRD measurements showed that peaks of ettringite, gypsum, and portlandite were observed in all the specimens. It can be seen from Fig. 9

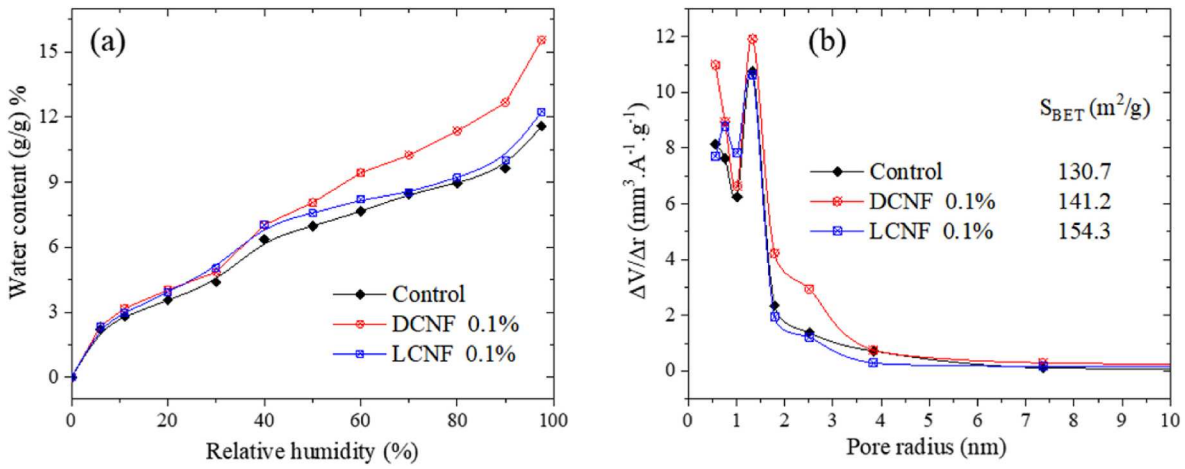

Fig. 7. (a) Water vapor desorption isotherms and (b) pore size distributions of the paste samples after 28 days of curing.

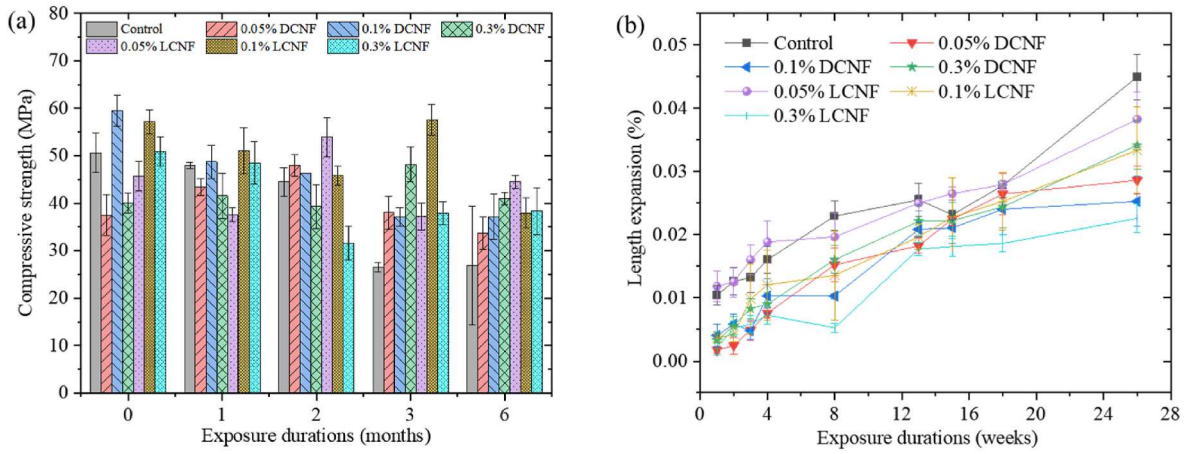

Fig. 8. (a) Compressive strengths and (b) Length change (expansion, %) of the mortar samples after Na_2SO_4 exposure.

Table 4
Change (%) in compressive strength and length of the mortar samples after 6 months of Na_2SO_4 exposure.

Sample ID	Change in compressive strength		Change in Length (expansion)
	w.r.t. control after 6 months	w.r.t. before exposure strength	w.r.t. control after 6 months
Control	–	−47.01	
DCNF 0.05%	+25.68	−10.11	−46.67
DCNF 0.10%	+38.39	−37.66	−47.88
DCNF 0.30%	+52.83	+2.58	−18.38
LCNF 0.05%	+66.08	+2.55	−25.25
LCNF 0.10%	+41.46	−33.62	−33.73
LCNF 0.30%	+42.91	−24.65	−50.9

that after the 6 months of Na_2SO_4 sulfate attack, the control specimen showed the lowest peak intensity of portlandite as compared to LCNF and DCNF specimens. This indicates that portlandite in the control specimen is being consumed to form ettringite and gypsum at a much higher rate than LCNF and DCNF specimens. Fig. 10 shows the DTG curves of specimens after 6 months of exposure to Na_2SO_4. The peak at around 120 °C is assigned to the dehydration of gypsum [44]. Similar to the observation from XRD, the gypsum formation appears to be the same for the LCNF and DCNF batches based on the DTG peaks. The portlandite content was slightly lower in the CNF-containing batches, which is due to the formation of calcium carbonate as observed from the DTG peak at around 600–700 °C. Among the CNF-containing specimens, LCNF registered higher amounts of C–S–H as compared to DCNF specimens. This is in good agreement with the observations made for length change. As observed from the pore size distribution analysis (Fig. 7), the addition of LCNF and DCNF leads to the densification of the cement matrix which can restricts the ingress of sulfate ions.

3.3. Role of LCNF and DCNF in resisting damage induced by $MgSO_4$

3.3.1. Macroscale effects

Fig. 11 (a) and (b) shows the compressive strengths and length changes (% expansion) of the mortar samples exposed to $MgSO_4$ solution. The % variations are reported in Table 5. For the control specimen, $MgSO_4$ was equally damaging as that of the Na_2SO_4, as observed by similar strength reduction after 6 months of exposure. However, the expansion of the mortar bars exposed to $MgSO_4$ was lesser compared to those of Na_2SO_4. When the sulfate solution interacts with the cement hydration products, the primary reaction products formed are gypsum and ettringite [52]. Furthermore, $MgSO_4$ exposure can cause decalcification of the main hydration product C–S–H gel, forming non-cementitious magnesium-silicate-hydrate (M-S-H) [52].

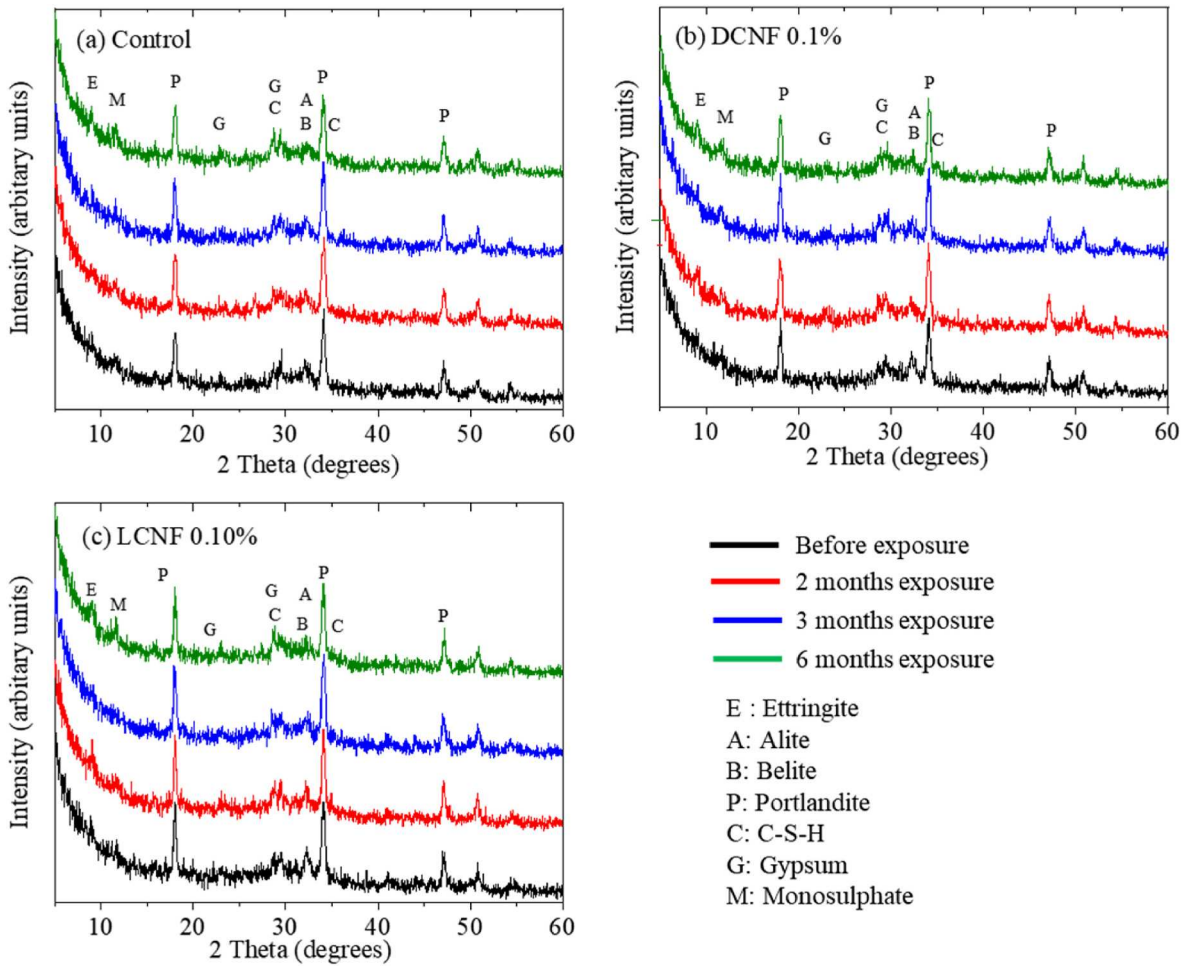

Fig. 9. XRD spectra of XRD spectra of (a) control (b) DCNF 0.10% (c) LCNF 0.10% specimens before and after 2, 3, and 6 months of Na_2SO_4 attack.

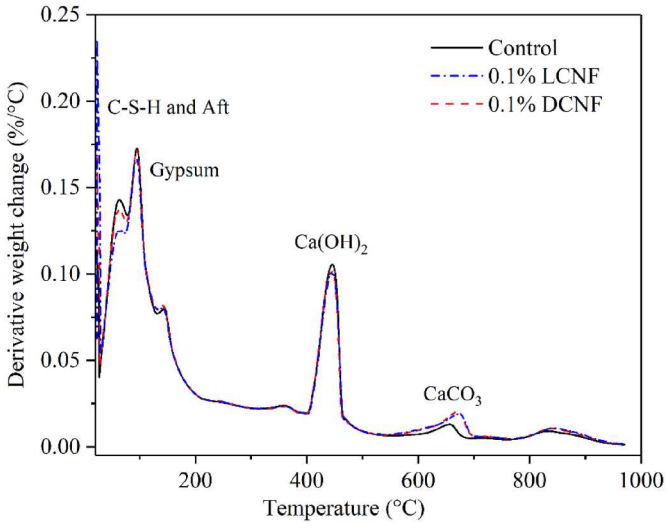

Fig. 10. DTG curves after 6 months of Na_2SO_4 attack.

Longitudinal expansion of mortar bars mainly occurs due to the formation of ettringite (Aft). Other reaction products like gypsum and M-S-H do not have expansive properties and can cause a loss of cohesive properties in the binder which ultimately results in the reduction of compressive strength. Therefore, the early stages of C–S–H degradation resulting in reduction of compressive strength are more evident than the gradual process of longitudinal expansion. As a result, the strength of the matrix is dropped without exhibiting any significant expansion. The addition of LCNF and DCNF improved the mortar's resistance to $MgSO_4$ attack. As observed from Table 5, the strength decreases of LCNF and DCNF-containing samples after 6 months of exposure to $MgSO_4$ was only around 25–30%, compared to the 46% decrease for the control batch. All the specimens containing any type of CNF showed significantly higher strength than that of the control batch after 6 months of exposure. After

Table 5
Change (%) in compressive strength and length of the mortar samples after 6 months of $MgSO_4$ exposure.

Sample ID	Change in compressive strength		Change in Length (expansion)
	w.r.t. control after 6 months	w.r.t. before exposure strength	w.r.t. control after 6 months
Control	–	−46.03	–
DCNF 0.05%	+72.80	+14.14	−3.87
DCNF 0.10%	+40.26	−28.40	−6.97
DCNF 0.30%	+42.86	−17.11	+12.66
LCNF 0.05%	+20.38	−25.29	−23.51
LCNF 0.10%	+74.35	+0.73	−26.36
LCNF 0.30%	+52.21	+22.53	−1.39

6 months of exposure, the compressive strength of the 0.1% DCNF specimen was 40% higher than that of the control specimen. In the case of the 0.1% LCNF specimen, the compressive strength was 74.3% higher than that of the control. It should be noted that LCNF specimens displayed better dimensional stability as compared to DCNF specimens when exposed to $MgSO_4$ solution as observed from the length change data (Fig. 11).

3.3.2. Microscale effects

The XRD spectra after 6 months of $MgSO_4$ exposure are shown in Fig. 12. Similar to the Na_2SO_4 exposure condition, the CNF-containing samples showed higher portlandite intensity. All of the batches showed nearly the same peak intensity for ettringite and monosulfate, indicating that sulfate diffused into the matrix for all samples after 6 months of exposure. The enhanced performance of CNF-containing batches could be due to the increased amounts of portlandite (resulted in a denser matrix) and the typical crack-bridging effects [23]. The DTG spectra of specimens exposed to $MgSO_4$ solution for 6 months is presented in Fig. 13. Both 0.1% DCNF and 0.1% LCNF specimens showed a higher presence of C–S–H phases than the control specimen. Moreover, the same observations were drawn for the portlandite phase as well for both LCNF and DCNF. This indicates that in LCNF and DCNF specimens, the portlandite phase is relatively safe from conversion to gypsum as compared to the control sample. Since gypsum softens the surface of the specimen it leads to lower compressive strength. As a result, the control sample showed a drastic reduction of compressive strength at the end of 6-month exposure. This behavior is true for both $MgSO_4$ and Na_2SO_4 sulfate attacks. The influence of LCNF in cement specimens exposed to sulfate attack presents an interesting observation. The LCNF specimens showed a higher amount of C–S–H in $MgSO_4$ exposed specimens than Na_2SO_4. This shows that LCNF specimens have high resistance to any form of sulfate attack.

3.4. Role of LCNF and DCNF in resisting damage induced by ASR

The interaction between cement and reactive aggregate leads to an alkali-silica reaction (ASR) which causes expansion cracks in cement composites [53]. The ASR severely reduces the service life of concrete [54]. The ability of CNF to mitigate ASR was investigated and is presented in Fig. 14. The mortar bars were first placed in the exposure condition as per the ASTM C 1260 [43] for 16 days. During this exposure duration, the length changes of the bars were measured every day. After this exposure duration, the mortar bars were kept in the same 1 N NaOH solution at room temperature (23 °C) for 1 year. After 1 year, the length changes of the bars were measured again. As observed from Fig. 14, the ASR-induced expansion was drastically reduced due to the addition of CNF. At the end of 16 days, the highest expansion of 0.21% was observed for the control specimen. Compared to the control specimen 0.3%DCNF sample recorded a decrease of 98.8% whereas 0.3%LCNF mix registered a decrease of 92.9% in expansion. For 0.1% dosage, the reductions in the expansion were 84% and 88% for the DCNF and LCNF-containing samples, respectively. After 1 year of exposure, while the control batch continued to expand, the CNF-containing samples did not show any further expansion. After 1 year of exposure, 0.1% DCNF and 0.1% LCNF samples showed around 89% and 97%, respectively, lower expansion compared to the control batch.

Cellulose nanofibers consist of negatively charged carboxyl and hydroxyl surface groups. The negatively charged surface attracts the positively charged alkali ions such as Na^+ and K^+ [24]. This attraction between the two oppositely charged ions leads to the binding of phases and reduces the availability of alkali ions for ASR. Since Akali ions get bound with the cellulose nanofibers the formation of ASR gel reduces. Similar to all other tested parameters, LCNF containing samples performed better against DCNF in the case of ASR resistance.

4. Discussion

It is well established that calcium ions in cement specimens are susceptible to sulfate attack. During the sulfate attack, hydrated cement matrix can form M-S-H, ettringite, and gypsum, which can contribute to the strength loss of the matrix [37]. Previous study reported that CNFs can enhance resistance of Portland cement composites against Na_2SO_4 by trapping calcium ions through electrostatic links [31]. $MgSO_4$ attack is usually more aggressive than Na_2SO_4 due to the formation of M-S-H and lowering of pH [55,56]. During this study, CNFs were found to be even more effective against $MgSO_4$ attack compared to the Na_2SO_4 attack. The positive effects of CNF in resisting sulfate damage were attributed to the microstructural densification due to the enhanced hydration, reinforcing effects, and calcium ion binding. Additionally, 0.1% LCNF-containing batch showed an increase in strength after exposure to Na_2SO_4 and $MgSO_4$ solutions for 3 months and 6 months, respectively. However, based on the XRD data (Figs. 9 and 12), any significant variation in mineral phase composition was not observed, i.e., the amounts of ettringite and gypsum consistently increased with exposure duration for all the batches (with and without CNF). Therefore, the strength variation with exposure duration is primarily due to the physical effects of CNF. Specifically, after an initial exposure duration (~3 months), cracks formed in the matrix, which enabled further intrusion of sulfate ions and increased the amounts of ettringite formation. In the control batch, the expansive nature of ettringite further degraded the strength of the mortar samples. Contradictorily, in CNF-containing samples, the expansive nature of ettringite is limited by the crack-bridging effects of

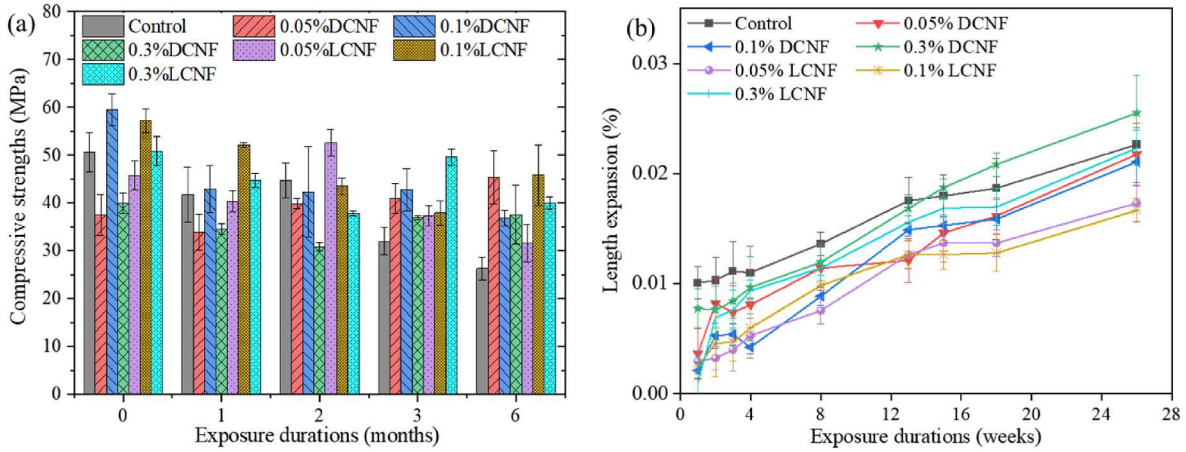

Fig. 11. (a) Compressive strengths and (b) Length change (expansion, %) of the mortar samples after $MgSO_4$ exposure.

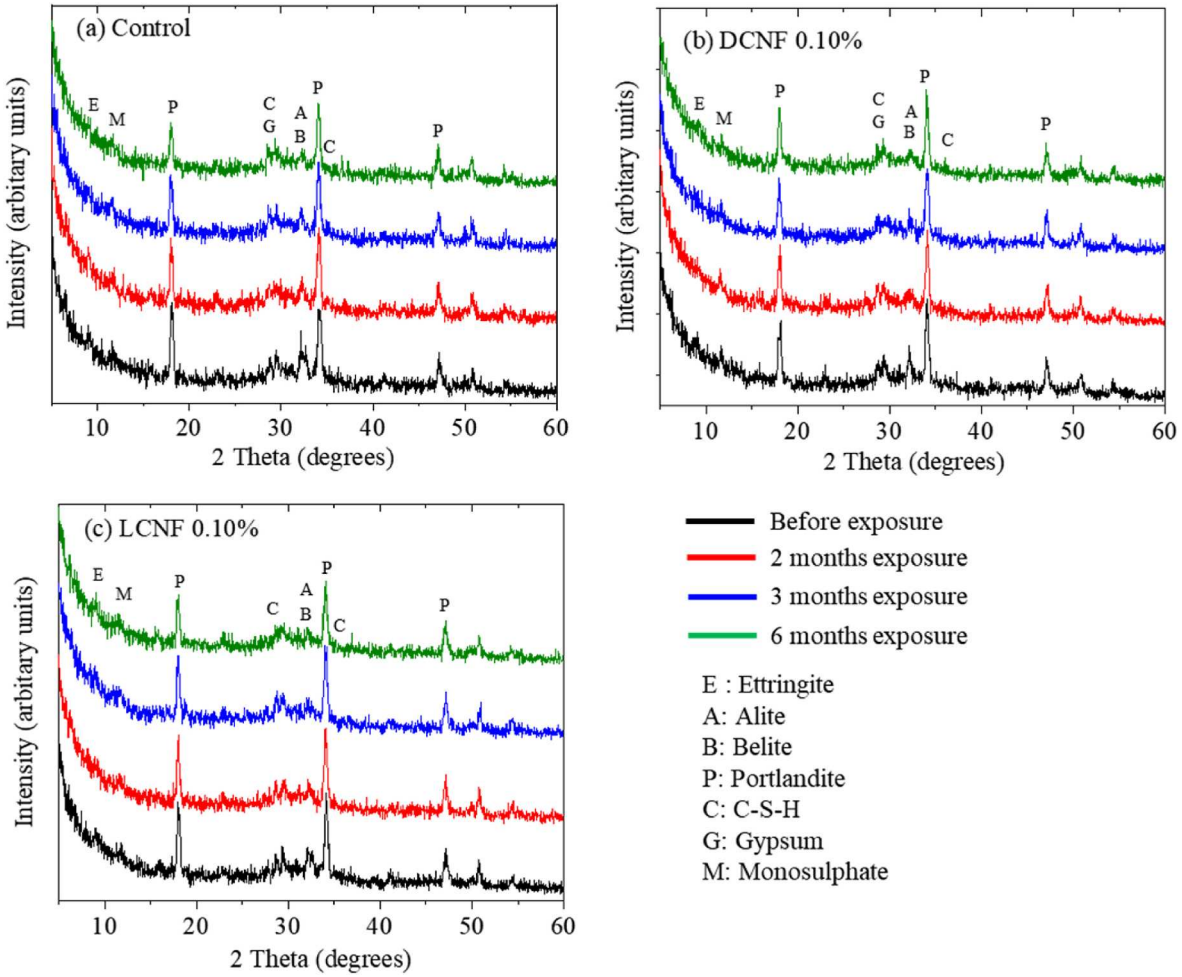

Fig. 12. XRD spectra of (a) control (b) DCNF 0.10% (c) LCNF 0.10% specimens before and after 2, 3, and 6 months of $MgSO_4$ attack.

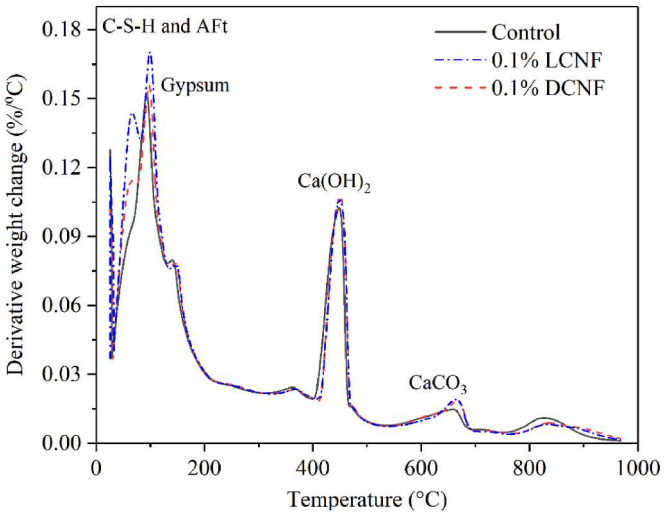

Fig. 13. DTG curves after 6 months of $MgSO_4$ attack.

CNF, and therefore, this ettringite formation results in densifications of the matrix. The increasing sulfate intrusion and expansive stress with exposure duration eventually cause the fibers to partially collapse and result in a strength loss after a long term exposure duration (i.e., 6 months).

Interestingly, both LCNF and DCNF were found to be highly effective in resisting the ASR damage of mortars after long-term exposure (1 year) in high alkaline environment. Cellulose fibers are known to be susceptible to alkaline degradation [57–59]. However, during such alkaline degradation process, cellulose binds alkali ions and form alkali cellulose, which is also addressed as alkaline cellulose nanofibrils in literature [60, 61]. Therefore, when LCNF and DCNF containing mortar samples with reactive aggregates were exposed to highly alkaline solution (1 N NaOH), the CNFs trapped the alkali ions through continuous alkali degradation process and prevented the formation of detrimental alkali silica reaction (ASR) gel. Specifically, 0.1% dosage of CNFs was observed to reduce the ASR expansion of the mortar bars by around 90% compared to the control batch. As such, CNFs can be an effective alternative to commercially available additives (e.g., lithium-based admixture or coal fly ash), which are typically used to reduce ASR damage of concrete.

For all the tested parameters, including 28-day compressive strength, nano-porosity, sulfate attack, and ASR resistance, LCNF was found to be more effective compared to DCNF. Important to note, lignin reduces the water demand of cement mixture and can be used as a plasticizer [62–64]. Additionally, the residual lignin can impart hydrophobicity to cellulose nanofibers [65]. In LCNF, both CNF and lignin are naturally intermixed at the nanoscale. As such, the hydrophobicity of lignin (i.e., plasticizer effect) contributes to the superior nanoscale dispersion of LCNF in cement paste compared to the DCNF. Such superior dispersion of LCNF resulted in the enhanced performance of LCNF-containing samples compared to those of DCNF as observed in this study. Therefore, the presence of lignin in CNF is advantageous for application in cementitious materials and can be considered a dispersion aid. In wood

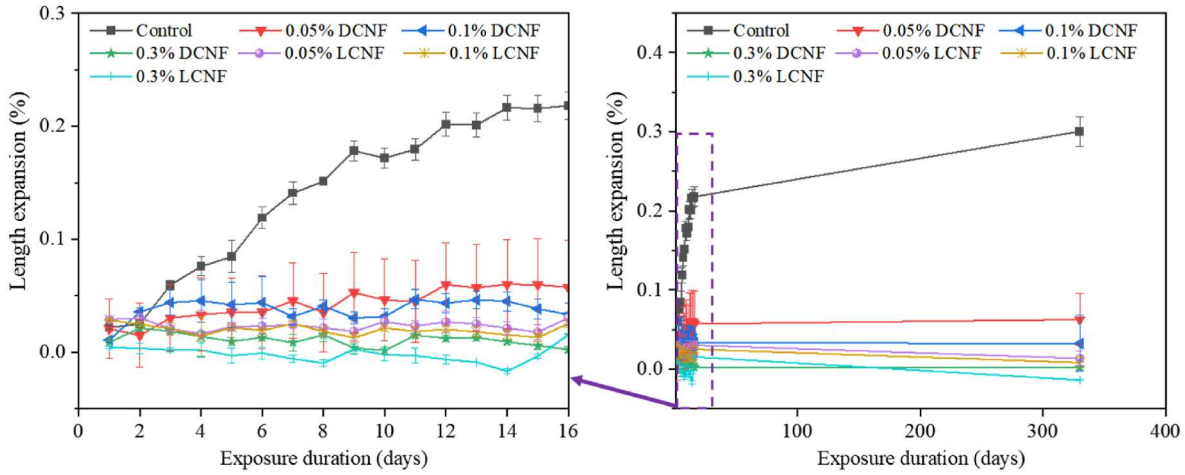

Fig. 14. Expansion due to alkali silica reaction.

pulps, lignin is naturally present with cellulose, and the production of DCNF involves the bleaching of wood pulp that generates lignin wastes. Accordingly, compared to DCNF, the utilization of LCNF in cementitious materials is not only scientifically advantageous but can also be a more economical and environmentally friendly pathway.

5. Conclusions

In the present study, the effectiveness of CNF in enhancing the resistance of mortar samples against sulfate attack and ASR damage was monitored for 6 months and 1 year, respectively. The following conclusions can be drawn.

1. The addition of CNF enhanced the isothermal heat evolution of cement. The enhanced hydration due to the addition of CNF was also evident from XRD and TGA results. From both XRD and TGA data, LCNF containing paste samples showed a higher amount of portlandite formation compared to the DCNF.
2. The pore size distribution analysis showed that CNF-containing samples have higher C–S–H contents compared to the control batch. However, the 0.1% LCNF-containing sample showed higher amounts of inner or high-density C–S–H formation, whereas the 0.1% DCNF-containing sample showed higher amounts of outer or low-density C–S–H.
3. The addition of up to 0.1% CNF into the cementitious system can reduce the expansion during the sulfate attack up to 47%. The nanofibers acted as a reinforcing agent which arrested the crack propagation and reduced the expansion.
4. Upon incorporating LCNF and DCNF into cement specimens, better resistance in terms of compressive strength was observed after exposure to $MgSO_4$ and Na_2SO_4 solution. 0.1% CNF containing samples was found to have up to 70% higher compressive strength than the control batch after 6 months of exposure to sulfate solution. The denser microstructure as well as the Ca^{2+} ion trapping mechanism of CNFs lead to better resistance against sulfate ingress.
5. The addition of CNF lowers the expansion of specimens due to ASR gel formation up to 97%. The alkali ion binding capacity of CNFs was the primary reason for lower ASR gel formation.

In summary, 0.1% CNF dosage is found to be optimum to enhance the durability performance of cementitious materials. For all the tested parameters, LCNF-containing samples showed better performance compared to DCNF samples. The superior performance of LCNF resulted from the increased amounts of high-density C–S–H in these samples compared to the DCNF. Due to the plasticizing effects of lignin, LCNF achieved a better nanoscale dispersion in cementitious materials compared to DCNF.

Declaration of competing interest

The authors declare that no conflict of interest is involved in this paper and the authors are responsible for the content and writing.

Data availability

Data will be made available on request.

Acknowledgment

This work was conducted with funding support from the U.S. Endowment for Forestry and Communities (P3Nano project # 21–00184) and National Science Foundation (NSF # ECI - 2028462) for Dr. Warda Ashraf. Dr. Surendra Shah appreciates the support of the Australian Reseach Council (IHI50100006). All opinions, findings, and conclusions or recommendations expressed in this material are those of the authors and do not necessarily reflect the views of the funding agencies.

References

[1] R.J. Moon, G.T. Schueneman, J. Simonsen, Overview of cellulose nanomaterials, their capabilities and applications, JOM 68 (2016) 2383–2394, https://doi.org/10.1007/s11837-016-2018-7.
[2] D. Ndahirwa, H. Zmamou, H. Lenormand, N. Leblanc, The role of supplementary cementitious materials in hydration, durability and shrinkage of cement-based materials, their environmental and economic benefits: a review, Clean. Mater. 5 (2022), https://doi.org/10.1016/j.clema.2022.100123.
[3] L. Laím, H. Caetano, A. Santiago, Review: effects of nanoparticles in cementitious construction materials at ambient and high temperatures, J. Build. Eng. 35 (2021), https://doi.org/10.1016/j.jobe.2020.102008.
[4] T.M. Sheikh, M.P. Anwar, K. Muthoosamy, J. Jaganathan, A. Chan, A.A. Mohamed, The mechanics of carbon-based nanomaterials as cement reinforcement — a critical review, Construct. Build. Mater. 303 (2021), https://doi.org/10.1016/j.conbuildmat.2021.124441.
[5] A.M. Onaizi, G.F. Huseien, N.H.A.S. Lim, M. Amran, M. Samadi, Effect of nanomaterials inclusion on sustainability of cement-based concretes: a comprehensive review, Construct. Build. Mater. 306 (2021), https://doi.org/10.1016/j.conbuildmat.2021.124850.
[6] M. Tabish, M.M. Zaheer, A. Baqi, Effect of nano-silica on mechanical, microstructural and durability properties of cement-based materials: a review, J. Build. Eng. 65 (2023), https://doi.org/10.1016/j.jobe.2022.105676.
[7] F. Matalkah, A. Ababneh, R. Aqel, Effects of nanomaterials on mechanical properties, durability characteristics and microstructural features of alkali-activated binders: a comprehensive review, Construct. Build. Mater. 336 (2022), https://doi.org/10.1016/j.conbuildmat.2022.127545.
[8] M.I. Haque, R.I. Khan, W. Ashraf, H. Pendse, Utilization of biochar as a multifunctional additive in cement-based materials, in: RILEM Bookseries, Springer Science and Business Media B.V., 2021, pp. 343–353, https://doi.org/10.1007/978-3-030-76551-4_31.

[9] M.I. Haque, R.I. Khan, W. Ashraf, H. Pendse, Production of sustainable , low-permeable and self-sensing cementitious composites using biochar, Sustain. Mater. Technol. 28 (2021), e00279, https://doi.org/10.1016/j.susmat.2021.e00279.

[10] J. Park, H. Suh, S.M. Woo, K. Jeong, S. Seok, S. Bae, Assessment of neutron shielding performance of nano-TiO2-incorporated cement paste by Monte Carlo simulation, Prog. Nucl. Energy 117 (2019), https://doi.org/10.1016/j.pnucene.2019.103043.

[11] I.M. Nikbin, R. Mohebbi, S. Dezhampanah, S. Mehdipour, R. Mohammadi, T. Nejat, Gamma ray shielding properties of heavy-weight concrete containing Nano-TiO2, Radiat. Phys. Chem. 162 (2019) 157–167, https://doi.org/10.1016/j.radphyschem.2019.05.008.

[12] F. Sanchez, K. Sobolev, Nanotechnology in concrete - a review, Construct. Build. Mater. 24 (2010) 2060–2071, https://doi.org/10.1016/j.conbuildmat.2010.03.014.

[13] K. Sobolev, I. Flores, R. Hermosillo, L.M. Torres-martínez, Nanomaterials and Nanotechnology for High-Performance Cement Composites, Symposium Paper, 2008, pp. 91–118. https://www.concrete.org/publications/internationalconcreteabstractsportal/m/details/id/20213. (Accessed 16 September 2023).

[14] Akira Isogai, Lennart Bergström, Preparation of cellulose nanofibers using green and sustainable chemistry, Curr. Opin. Green Sustainable Chem. 12 (2018) 15–21.

[15] L. Oliveira de Souza, M. Cordazzo, L.M. Silva de Souza, G. Tonoli, F. de Andrade Silva, V. Mechtcherine, Investigation of dispersion methodologies of microcrystalline and nano-fibrillated cellulose on cement pastes, Cem. Concr. Compos. 126 (2022), https://doi.org/10.1016/j.cemconcomp.2021.104351.

[16] Q. Fan, X. Meng, Z. Li, G. Ma, Z. Wang, K. Zhang, C. He, D. Meng, Experiment and molecular dynamics simulation of functionalized cellulose nanocrystals as reinforcement in cement composites, Construct. Build. Mater. 341 (2022), https://doi.org/10.1016/j.conbuildmat.2022.127879.

[17] A.D. Çavdar, H. Yel, S.B. Torun, Microcrystalline cellulose addition effects on the properties of wood cement boards, J. Build. Eng. 48 (2022), https://doi.org/10.1016/j.jobe.2021.103975.

[18] J.A. Oh, M. Aakyiir, Y. Liu, A. Qiu, T.R. Meola, P. Forson, S. Araby, Y. Zhuge, S. H. Lee, J. Ma, Durable cement/cellulose nanofiber composites prepared by a facile approach, Cem. Concr. Compos. 125 (2022), https://doi.org/10.1016/j.cemconcomp.2021.104321.

[19] L. Jiao, M. Su, L. Chen, Y. Wang, H. Zhu, H. Dai, Natural cellulose nanofibers as sustainable enhancers in construction cement, PLoS One 11 (2016), https://doi.org/10.1371/journal.pone.0168422.

[20] S. Parveen, S. Rana, R. Fangueiro, M.C. Paiva, A novel approach of developing micro crystalline cellulose reinforced cementitious composites with enhanced microstructure and mechanical performance, Cem. Concr. Compos. 78 (2017) 146–161, https://doi.org/10.1016/j.cemconcomp.2017.01.004.

[21] K.S. Kamasamudram, W. Ashraf, E.N. Landis, R.I. Khan, Effects of ligno– and delignified– cellulose nanofibrils on the performance of cement-based materials, J. Mater. Res. Technol. 13 (2021) 321–335, https://doi.org/10.1016/j.jmrt.2021.04.090.

[22] K.S. Kamasamudram, W. Ashraf, E.N. Landis, Cellulose Nanocomposites for Performance Enhancement of Ordinary Portland Cement-Based Materials, Transportation Research Record: Journal of the Transportation Research Board, Nanotechno, 2020, https://doi.org/10.1177/0361198120958421.

[23] K.S. Kamasamudram, W. Ashraf, E.N. Landis, Cellulose nanofibrils with and without nanosilica for the performance enhancement of portland cement system, Construct. Build. Mater. 285 (2021).

[24] M.I. Haque, W. Ashraf, R.I. Khan, S. Shah, A comparative investigation on the effects of nanocellulose from bacteria and plant-based sources for cementitious composites, Cem. Concr. Compos. 125 (2022), https://doi.org/10.1016/j.cemconcomp.2021.104316.

[25] O. Onuaguluchi, N. Banthia, Plant-based natural fibre reinforced cement composites: a review, Cem. Concr. Compos. 68 (2016) 96–108, https://doi.org/10.1016/j.cemconcomp.2016.02.014.

[26] S.J. Peters, T.S. Rushing, E.N. Landis, T.K. Cummins, Nanocellulose and microcellulose fibers for concrete, Transport. Res. Rec. (2010) 25–28, https://doi.org/10.3141/2142-04.

[27] H.H. Kolour, W. Ashraf, E.N. Landis, Hydration and early age properties of cement pastes modified with cellulose nanofibrils, in: Transp Res Rec, SAGE Publications Ltd, 2021, pp. 38–46, https://doi.org/10.1177/0361198120945993.

[28] H.H. Kolour, M. Ahmed, E. Alyaseen, E.N. Landis, An investigation on the effects of cellulose nanofibrils on the performance of cement paste and concrete, Adv. Civ. Eng. Mater. 7 (2018) 463–478, https://doi.org/10.1520/ACEM20180048.

[29] O. Onuaguluchi, D.K. Panesar, M. Sain, Properties of nanofibre reinforced cement composites, Construct. Build. Mater. 63 (2014) 119–124, https://doi.org/10.1016/j.conbuildmat.2014.04.072.

[30] Y. Cao, P. Zavaterri, J. Youngblood, R. Moon, J. Weiss, The influence of cellulose nanocrystal additions on the performance of cement paste, Cem. Concr. Compos. 56 (2015) 73–83, https://doi.org/10.1016/j.cemconcomp.2014.11.008.

[31] J. Goncalves, M. El-Bakkari, Y. Boluk, V. Bindiganavile, Cellulose nanofibres (CNF) for sulphate resistance in cement based systems, Cem. Concr. Compos. 99 (2019) 100–111, https://doi.org/10.1016/j.cemconcomp.2019.03.005.

[32] J. Goncalves, Y. Boluk, V. Bindiganavile, Cellulose nanofibres mitigate chloride ion ingress in cement-based systems, Cem. Concr. Compos. 114 (2020), https://doi.org/10.1016/j.cemconcomp.2020.103780.

[33] M. Santhanam, M. Cohen, J. Olek, Differentiating seawater and groundwater sulfate attack in Portland cement mortars, Cement Concr. Res. 36 (2006) 2132–2137, https://doi.org/10.1016/j.cemconres.2006.09.011.

[34] J. Cao, Q. Ding, D. Hou, C. Xiong, Z. Jin, G. Zhang, Influence of hoop restraint on microstructure and phase composite of cement paste filled steel tube under external sulfate attack, Construct. Build. Mater. 366 (2023), https://doi.org/10.1016/j.conbuildmat.2022.130195.

[35] M.E.G. Dobrovolski, G.S. Munhoz, E. Pereira, R.A. Medeiros-Junior, Effect of crystalline admixture and polypropylene microfiber on the internal sulfate attack in Portland cement composites due to pyrite oxidation, Construct. Build. Mater. 308 (2021), https://doi.org/10.1016/j.conbuildmat.2021.125018.

[36] E. Pereira, E. Pereira, S.A. Pianaro, M.M. Farias, M.D.O.G.P. Bragança, I. C. Oliveira, Combined effect of alkali-aggregate reaction (AAR) and internal sulfate attack (ISA): microstructural and porous structure modifications of portland cement mortars, Construct. Build. Mater. 362 (2023), https://doi.org/10.1016/j.conbuildmat.2022.129676.

[37] A. Neville, The confused world of sulfate attack on concrete, Cement Concr. Res. 34 (2004) 1275–1296, https://doi.org/10.1016/j.cemconres.2004.04.004.

[38] ASTM C 150, Standard Specification for Portland Cement, vol. 1, 2007, https://doi.org/10.1520/C0150_C0150M-19.

[39] ASTM C778, Standard Specification for Standard Sand, 2021, https://doi.org/10.1520/C0778-21.

[40] X. Zhang, L. Zhang, Y. Fan, Z. Wang, The Case-dependent Lignin Role in Lignocellulose Nanofibers Preparation and Functional Application-A Review, Green Energy and Environment, 2022, https://doi.org/10.1016/j.gee.2022.09.008.

[41] O. Onuaguluchi, N. Banthia, Sulfate resistance of cement composites containing Nano-Fibrillated Cellulose (NFC), Cem. Concr. Compos. 135 (2023), https://doi.org/10.1016/j.cemconcomp.2022.104831.

[42] ASTM C1012, Standard Test Method for Length Change of Hydraulic-Cement Mortars Exposed to a Sulfate Solution, 2018, https://doi.org/10.1520/C1012_C1012M-18B.

[43] ASTM C1260, Standard Test Method for Potential Alkali Reactivity of Aggregates, Mortar-Bar Method, 2022, https://doi.org/10.1520/C1260-22.

[44] K. Scrivener, R. Snellings, B. Lothenbach, A Practical Guide to Microstructural Analysis of Cementitious Materials, first ed., CRC Press, 2017.

[45] ASTM C109, Standard Test Method for Compressive Strength of Hydraulic Cement Mortars (Using 2-in. Or [50-mm] Cube Specimens), 2020, https://doi.org/10.1520/C0109_C0109M-20B.

[46] ASTM C157: Standard Test Method for Length Change of Hardened Cement Mortar And Concrete, https://doi.org/10.1520/C0157_C0157M-08R14E01.

[47] T. Fu, F. Montes, P. Suraneni, J. Youngblood, J. Weiss, The influence of cellulose nanocrystals on the hydration and flexural strength of Portland cement pastes, Polymers 9 (2017), https://doi.org/10.3390/polym9090424.

[48] E.P. Barrett, L.G. Joyner, P.P. Halenda Vol, R. -RnAtn Apj, R.A. Vn-Rn Atn Ac, Vp2 = R2AV2-R2at2 ACi Generalizing Equation (4) and Substituting (6a) for Vm* Yields, n.d.

[49] W. Ashraf, J. Olek, Elucidating the accelerated carbonation products of calcium silicates using multi-technique approach, J. CO2 Util. 23 (2018) 61–74, https://doi.org/10.1016/j.jcou.2017.11.003.

[50] S. Brunauer, P.H. Emmett, E. Teller, Adsorption of Gases in Multimolecular Layers, 1938. https://pubs.acs.org/sharingguidelines.

[51] V. Baroghel-Bouny, Water vapour sorption experiments on hardened cementitious materials. Part I: essential tool for analysis of hygral behaviour and its relation to pore structure, Cement Concr. Res. 37 (2007) 414–437, https://doi.org/10.1016/j.cemconres.2006.11.019.

[52] M. Santhanam, M.D. Cohen, J. Olek, Sulfate attack research - whither now? Cement Concr. Res. 31 (6) (2001) https://doi.org/10.1016/S0008-8846(01)00510-5.

[53] M. Kasaniya, M.D.A. Thomas, Role of the alkalis of supplementary cementing materials in controlling pore solution chemistry and alkali-silica reaction, Cement Concr. Res. 162 (2022), https://doi.org/10.1016/j.cemconres.2022.107007.

[54] T.N. Nguyen, L.F.M. Sanchez, J. Li, B. Fournier, V. Sirivivatnanon, Correlating alkali-silica reaction (ASR) induced expansion from short-term laboratory testings to long-term field performance: a semi-empirical model, Cem. Concr. Compos. 134 (2022), https://doi.org/10.1016/j.cemconcomp.2022.104817.

[55] Lea's Chemistry of Cement and Concrete, Elsevier, 2019, https://doi.org/10.1016/C2013-0-19325-7.

[56] M. Wu, Y. Zhang, Y. Ji, W. She, L. Yang, G. Liu, A comparable study on the deterioration of limestone powder blended cement under sodium sulfate and magnesium sulfate attack at a low temperature, Construct. Build. Mater. 243 (2020), https://doi.org/10.1016/j.conbuildmat.2020.118279.

[57] M.A. Glaus, L.R. Van Loon, Cellulose Degradation at Alkaline Conditions: Long-Term Experiments at Elevated Temperatures, Paul Scherrer Institute, 2004. www.psi.ch.

[58] M.A. Glaus, L.R. Van Loon, Degradation of cellulose under alkaline conditions: new insights from a 12 years degradation study, Environ. Sci. Technol. 42 (2008) 2906–2911, https://doi.org/10.1021/es7025517.

[59] I. Pavasars, J. Hagberg, H. Borén, B. Allard, Alkaline degradation of cellulose: mechanisms and kinetics, J. Polym. Environ. 11 (2003) 39–47.

[60] J. Gu, Y. Lo Hsieh, Alkaline cellulose nanofibrils from streamlined alkali treated rice straw, ACS Sustain. Chem. Eng. 5 (2017) 1730–1737, https://doi.org/10.1021/acssuschemeng.6b02495.

[61] A.T. Serkov, Fabrication of alkali cellulose, Fibre Chem. 32 (2) (2000).

[62] D. Robert, Effects of Lignin-Based Admixtures on Time Dependent Volume Changes in Concrete, Thesis, The University of New South Wales, 1997, https://doi.org/10.26190/unsworks/9260.

[63] A. Ur, R. Akond, Application of Lignin (Modified/Unmodified) to Cement and Observing Effects Observing Effects, Thesis, Louisiana Tech University, 2020, https://digitalcommons.latech.edu/theses.
[64] P. Jędrzejczak, M.N. Collins, T. Jesionowski, Ł. Klapiszewski, The role of lignin and lignin-based materials in sustainable construction – a comprehensive review, Int. J. Biol. Macromol. 187 (2021) 624–650, https://doi.org/10.1016/j.ijbiomac.2021.07.125.
[65] Y. Jiang, X. Liu, Q. Yang, X. Song, C. Qin, S. Wang, K. Li, Effects of residual lignin on composition, structure and properties of mechanically defibrillated cellulose fibrils and films, Cellulose 26 (2019) 1577–1593, https://doi.org/10.1007/s10570-018-02229-4.